Iraqi National Journal of Earth Science

www.earth.mosuljournals.com

Geochemical Parameters for Evaluating the Aptian-Albian Kaolin Deposits at Abu Darag Region, Gulf of Suez: Implications for the Paleoclimatic Conditions in the Depositional Environments

Hatem M. El-Desoky[1], Mohamed W. Abd El Moghny[2] , Nabil A. Abdel Hafez[3], Osama R. El-Shahat[4], Sherif Farouk[5], Hossam K. Sharaka[6]

[1,2,3,4] Department of Geology, Faculty of Science, Al-Azhar University, Egypt.
[5] Department Exploration, Egyptian Petroleum Research Institute (EPRI), Egypt.
[6] Egyptian Mineral Resources Authority (EMRA), Egypt.

Article information

Received: 13- Aug -2022

Accepted: 27- Nov -2022

Available online: 31-Dec-2022

Keywords:
Genesis
Paleo-weathering
Climatic constraint
Abu Darag
Wadi Araba
Egypt

Correspondence:
Name: Hossam K. Sharaka
hossam.sharaka_2014@yahoo.com

ABSTRACT

The mineralogical and geochemical constituents of the Aptian-Albian Malha Formation at the Abu Darag region, Gulf of Suez, Egypt, can be discussed here. These constituents are related to paleoweathering and paleoclimatic circumstances that managed the depositional settings. The present study aims to evaluate the geochemical conditions that have control over the depositional environments and characterizes them in terms of lithological, mineralogical, and chemical composition. To achieve this aim, selected kaolinitic clay samples were geochemically and mineralogically examined. Kaolinite and quartz are the main constituent minerals in the investigated samples, whereas anatase and hematite serve as auxiliary minerals. The presence of hematite minerals indicates precipitation in an oxidizing environment, whereas anatase is related to basaltic rock. Bivariate discrimination provenance diagrams, major oxides, and trace elements all identify felsic-intermediate igneous source rocks as the leading contenders. The examined samples were deposited in non-marine environments and underwent weak to moderate chemical weathering as well as severe physical induration in tropical climates.

DOI: 10.33899/earth.2022.135180.1025,

المعاملات الجيوكيميائية لتقييم رواسب الكاولين الأبتيان– البيان في منطقة أبو الدرج، خليج السويس: الإنعكاسات على الظروف المناخية القديمة في بيئات الترسيب

حاتم الدسوقي [1]، محمد وجية عبدالمغني [2]، نبيل علي عبدالحافظ [3]، اسامة رمزي الشحات [4]،
شريف فاروق [5]، حسام الدين خيري حسين شراقة [6]
[1، 2، 3، 4] قسم علوم الأرض، كلية العلوم، جامعة الأزهر، مصر.
[5] قسم الإستكشاف، معهد بحوث البترول، مصر.
[6] قسم الإستكشاف، هيئة المساحة الجيولوجية، مصر.

معلومات الارشفة

تاريخ الاستلام: 13- أغسطس-2022

تاريخ القبول: 27- نوفمبر-2022

تاريخ النشر الالكتروني: 31-ديسمبر-2022

الكلمات المفتاحية:
النشأة
التجوية القديمة
التحكم في المناخ
أبو الدرج
وادى عربة
مصر

المراسلة:
الاسم: حسام الدين خيري حسين
hossam.sharaka_2014@yahoo.com

الملخص

يهدف البحث الحالي الى معرفة المكونات المعدنية والجيوكيميائية لمكون المالحة Aptian-Albian في منطقة أبو الدرج، خليج السويس، مصر. حيث وجد أن هذه المكونات ترتبط بالتجوية الكيميائية والظروف المناخية القديمة والتي ساهمت في إعادة الترسيب. تهدف الدراسة الحالية إلى تقييم الظروف الجيوكيميائية التي تتحكم في بيئات الترسيب وتميزها من حيث التركيب الصخري المعدني والكيميائي. ولتحقيق هذا الهدف، تم فحص عينات من الطين الكوالييني جيوكيميائيا ومعدنيا، حيث وجد أن الكاولينيت والكوارتز من المعادن الرئيسية في العينات التي تم فحصها، بينما يتواجد anatase وhematite كمعادن إضافية. يشير وجود معدن الهيماتيت إلى أن هذه العينات ترسبت في بيئة مؤكسدة، بينما يشير anatase إلى الصخور البازلتية. تحدد الرسوم البيانية لمصدر التمييز ثنائي المتغير، والأكاسيد الرئيسية، والعناصر النادرة إلى أن صخور المصدر ترجع إلى الصخور الحامضية والمتوسطة في النشأة. وقد خضعت العينات المفحوصة لعوامل التجوية الكيميائية الخفيفة إلى المعتدلة بالإضافة إلى الترسيب في الظروف المناخية المدارية والتي ترسبت في بيئات غير بحرية.

DOI: 10.33899/earth.2022.135180.1025,

Introduction

The chemical and mineralogical characteristics of clastic sedimentary rocks can be used to determine the depositional environment and the provenance based on several factors. These are including the composition of their source rocks, environmental factors influencing the weathering of source rocks (atmospheric chemistry, temperature, rainfall, and topography), the duration of weathering, and transportation mechanisms of clastic material from the source region to the depositional area (Hayashi, et al., 1977). The primary controlling factors that influence the geochemistry of clastic sedimentary rocks are lithology, mineral composition, chemical weathering, and post-depositional change during diagenesis of the source locations are reported by Johnsson (1993) and Armient, et al. (1998). Furthermore, these parameters are influenced by tectonic activity, source fluctuations, climatic changes, and sediment quality. (Álvarez, 2005). As a result, major and trace elements can be used to determine how climate influenced clastic deposit deposition and weathering (Barbera, et al., 2006).

Bauxites, laterites, and altered metamorphic and igneous rocks are just a few examples of the diverse lithologies that can host kaolin deposits, which can also occur in a variety of depositional environments, including tropical soils and floodplain deposits (Dill, et al., 1997). To distinguish between hypogenic and supergene kaolinization processes, they employed the (Cr + Y + La)/ (Ba + Sr) and P/S, Zr/Ti, and (Cr + Nb)/ (Ti + Fe) ratios. The origin of kaolin deposits is related to widely different geochemical environments, such as hydrothermal alteration (primary), weathering (residual and leaching), sedimentary (secondary), and

crystallization from colloids having the chemical composition of kaolinite (Youssef, 1996; Wilson, 2004). The formation of kaolinite in association with free oxides and hydrated oxides of aluminum, iron, and titanium is the characteristic of lateritic weathering in humid tropical and sub-tropical zones. Moreover, in dry seasons, in tropical regions, aluminum hydroxide precipitated from the clay minerals in an insoluble form and accumulates at or near the surface as kaolin. Geoscientists have been paying close attention to the geochemistry of kaolin deposits to better understand the processes at work in these sediments, including their origin, and natural processes, along with a summary of the major and trace element distribution in these sediments. (Zhang, et al., 2001).

According to Khoury (2002) and Khoury, et al. (2008), claystone that is smaller than 2 m in size frequently contains a mixture of various rock fragments and clay minerals. The most widespread clay mineral is called kaolinite, and it is a 1:1 layered silicate made up of alternating layers of $[Si_2O_5]_2$- and $[Al_2(OH)_4]_2$+. $Si_2Al_2O_5(OH)_4$ is the theoretical formula for kaolinite (frequently expressed as $Al_2O_3.2SiO_2.2H_2O$). Kaolinite is found in kaolin deposits alongside other clay minerals such as smectite and illite (Correia, et al., 2005). Secondary sedimentary kaolin deposits are composed of sedimentary clay-rich rocks, while primary kaolin deposits were formed in situ by modification of igneous and/or metamorphic protoliths. Many different lithologies including kaolinite produce kaolin deposits (e.g., Murray and Keller, 1993; Pruett and Pickering, 2006; Murray, 2007).

The studied kaolin deposits are visible as well-developed intercalated layers in the Early Cretaceous Malha Formation, rising to 2.4 meters. The reserves of sedimentary kaolin deposits of the Abu Darag district, reach up to >54 Mt. Investigating how the exposed kaolin deposits in the Abu Darag region, were formed is the goal of the current study. The study area lies between longitudes 32°00' and 32°35' east and latitudes 29°00' to 29°35' north (Fig. 1).

Geological Outline

The exposed section was investigated in the Abu Darag region, which is a few kilometers west of the asphalt Suez-Zaafarana route and about 125 kilometers south of Suez City. Furthermore, the asphalt Suez-Ras Gharib road's Wadi Araba stretch lies 52 kilometers to the west of it (Fig. 1).

The Northern and Southern Galalah Plateaus, as well as the upstream section of Wadi Qena, are excellent locations for exposing the Malha Formation (Abdallah and Adindani, 1963). Wadi Malha, on the western shore of the Gulf of Suez, is the type locality of the formation officially known as the 'Malha Formation' that was reported by Abdallah and Adindani (1963).

Different lithological rock units with ages ranging from Carboniferous to Eocene are present in the area under study and are covered by Quaternary deposits as shown in the geologic map (Fig. 1). The Aptian-Albian Malha Formation represents a predominantly clastic facies sedimentation in the area. The studied kaolin deposits intercalated within the varicolored sandstone which is related to the Malha Formation. In the studied region, a wavy continuous unconformity denotes the lower contact between the Malha Formation and the Qiseib Formation underneath it. This contact is shown by a band of paleosols, while the upper contact with the Galala Formation underneath it is indicated by an uneven continuous unconformity.

The sandstone of the Malha Formation is moderately hard to hard, planar, and tabular cross-bedding with iron oxide patches. The studied successions were formed mainly of thick clay, and sandstone was found as layers free of any calcareous material or fossils (Fig. 2). This sandstone bed is intercalated with thick laminated kaolinitic clays, ranging in color from grey-yellow to reddish. The studied district is close to the basement rocks that are rich in feldspar minerals.

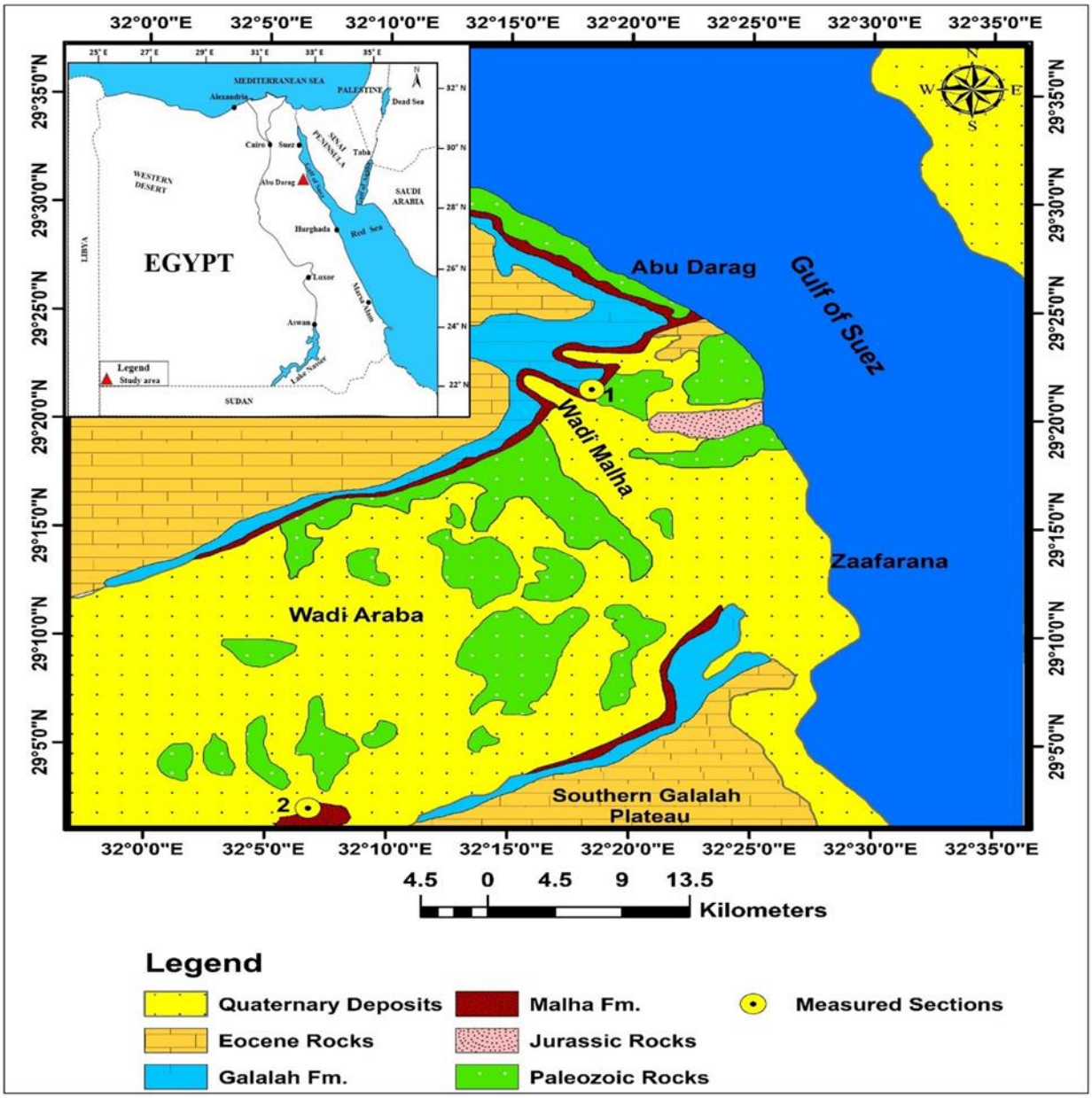

Fig. 1. Location and geological map of Abu Darag district, western side of the Gulf of Suez, Red Sea (Modified after Scheibner, et al., 2003).

Materials and Methods

To determine their mineralogical and geochemical features, 26 samples were taken from three exposed sections. The chosen samples were evaluated using a Philips-type PANalytical Equipment Model X-Pert-PRO automated powder diffractometer system with a Ni-filter, a Cu-radiation (=1.542) of 45 kV, and 35 mA. The peak of the reflection occurs between 2o and 60o. High Score Plus software was used to control the generator, and the PDF/ICCD database was utilized to enable peak recognition. Using a model "Philips Pw/2404" of 30 kW, X-ray fluorescence (XRF) analysis was utilized to evaluate the chemical content of the primary oxides and trace elements in the selected claystone samples. XRD and XRF tests were carried out at the central laboratory division of the Egyptian Geological Survey in Cairo, Egypt.

The selected major and trace elements were standardized to the upper continental crust (UCC; Taylor and McLennan, 1985) to differentiate between the composition of the source rocks and the trend of elemental fluctuations relative to the UCC. The Post-Achaean Australian Shale (PAAS) values were also utilized for comparison when it was practical.

Ternary (A-CN-K and A-CNK-FM) diagrams were provided by Nesbitt and Young (1984, 1989) to understand their mineralogical constituents and weathering trends. To estimate the chemical maturity trend as a function of climate, a bivariate diagram is used to plot SiO2 against Al_2O_3 + Na_2O + K_2O, among other variables (Suttner and Dutta, 1986). Additionally, chemical maturity can be determined using the ternary ($5Al_2O_3$-SiO_2-2CaO) diagram (Brumsack, 1989). Roaldest (1978) introduced the link between (K_2O/Al_2O_3) against (MgO/Al_2O_3) to distinguish between marine and non-marine deposits.

SiO_2 vs. log (K_2O/Na_2O) and (Zr vs Ti) plots can be used to determine the tectonic background and unknown genesis of kaolin deposits (Hayashi, et al., 1977; Roser and Korsch, 1986, respectively). The ratio of Al_2O_3 to TiO_2 was plotted to ascertain the makeup of the source rocks (Hayashi, et al., 1977). A scattered plot (Al_2O_3-SiO_2-Fe_2O_3) ternary diagram is used to assess the degree of kaolinization (Aleva, 1994). The degree to which feldspar has been transformed into aluminous weathering products is determined by the chemical index of alteration (Nesbitt and Young, 1982, 1984). The plagioclase index of alteration can be used to quantify diagenesis-related source area weathering and elemental redistribution. This indicator can be utilized to determine the degree of chemical reactions and was modified from the CIA equation to monitor plagioclase (Fedo, et al., 1995).

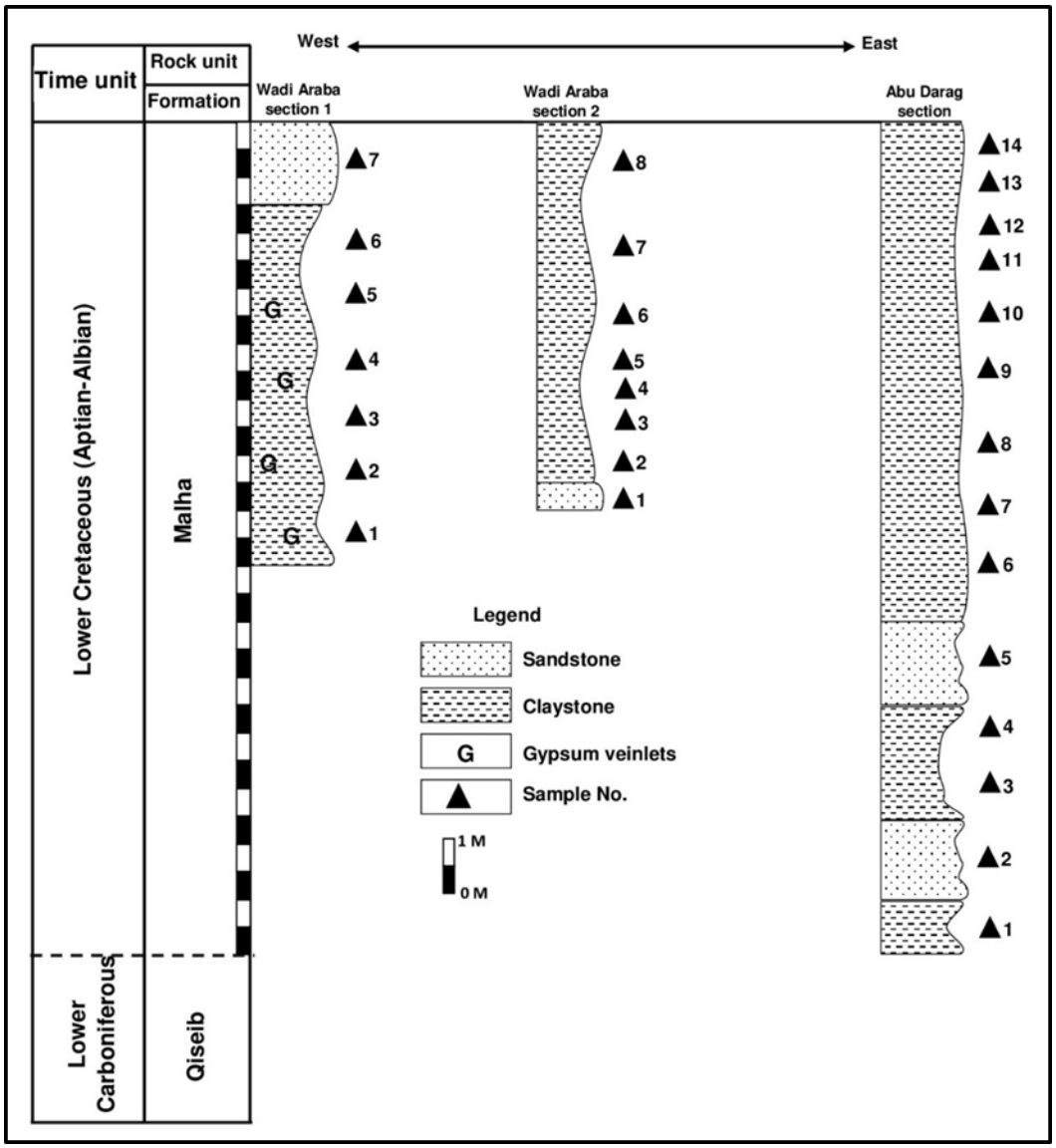

Fig. 2. Lithostratigraphic columnar sections of the Lower Cretaceous sedimentary sequence in the Abu Darag area, western side of the Gulf of Suez (Abu Darag and Wadi Araba 1 and 2).

Results

Field geology

The Lower Cretaceous clastic beds of the Malha Formation in the Abu Darag region, are made up of ferruginous, trough cross-bedded sandstones. In the alternative, together with green silty shales and kaolin interbeds, which were more common in the lower section of the formation. Numerous major and minor faults with lengths ranging from a few meters to 10 kilometers and a dominant direction. Lines are running NW-SE close to the Gulf of Suez in this region (Fig. 1). The Malha Formation rests erratically on the Qiseib Formation in the research region (Lower Carboniferous, Fig. 2; Farouk 2016). The Galala Formation lies unconformably above the Malha Formation with sharp vertical facies changes. It consists of calcareous mudstones, shale, and thin layers of fossiliferous limestone. The kaolin deposits' thickness varied in the study area from 1 to 10 meters. In another word, the existence of a ferruginous sandstone bed that forms the marked bed between the kaolin thin layer and their overlying sandstones distinguishes the upper surface of the kaolin beds. The examined successions are primarily composed of thick strata of clay and sandstone that do not include any calcareous material (Figs. 2 and 3). The lower bed is composed of cross-bedding and thin-lamination fine, medium, and coarse-grained sandstones. This sandstone deposit contains kaolinitic clays that range in color from grey-yellow to reddish. A dense, layered sequence of red color distinguishes the clayey strata.

Mineral composition

The x-ray diffraction analysis demonstrates that the examined kaolin samples are mostly made of the mineral's quartz and kaolinite, with minor amounts of accessory minerals (e.g., hematite, albite, gypsum, and anatase; Fig. 4). The non-clay (quartz) mineral is found as detrital grains that are the result of the Pre-Cambrian basement rocks' chemical weathering. Gypsum can only be seen in the Wadi Araba section, where it is a minor mineral in the bottom portion of the sample (WA2) and a large ingredient in the top part (WA8) (Figs. 3 and 4). In all the samples that were examined, hematite was listed as a small component (Fig. 4). Albite is found as a minor component mineral in the Wadi Araba section (samples WA1, WA2, WA3, WA5, WA6, and WA8) and the Abu Darag region (samples AD1, AD2, AD9, AD10, and AD11) (Fig. 4). On the other hand, XRD shows that kaolinite is the main clay mineral in the samples under investigation (Fig. 4).

Geochemical behavior of elements

The geochemical characteristics of the samples under investigation were evaluated using XRF techniques to ascertain the distribution of both the significant oxides and trace elements. These results showed that the examined samples were made up of major oxides (SiO_2 and Al_2O_3) as significant constituents, while trace oxides (MgO, Cl, P_2O5, and SO_3) and alkali elements (e.g., CaO, Na_2O, and K_2O) were also present and came from various sources (Table 1).

The average SiO2 concentration (57.24%) is lower than several other works' median frequencies (e.g., Gromet, et al., 1984; Taylor and McLennan, 1985; Condie, 1993; Sayin, 2007; Okunlola and Idowu, 2012; Grecco et, al., 2012) that were provided in Table (2). Additionally, the average Al_2O_3 concentration was lower (23.51%) than that of (Montes, et al., 2002; Wilson, 2004; Baioumy and Gilg, 2011; Khater, et al., 2013; Saber, et al., 2018; El Nagar and Khater, 2019).

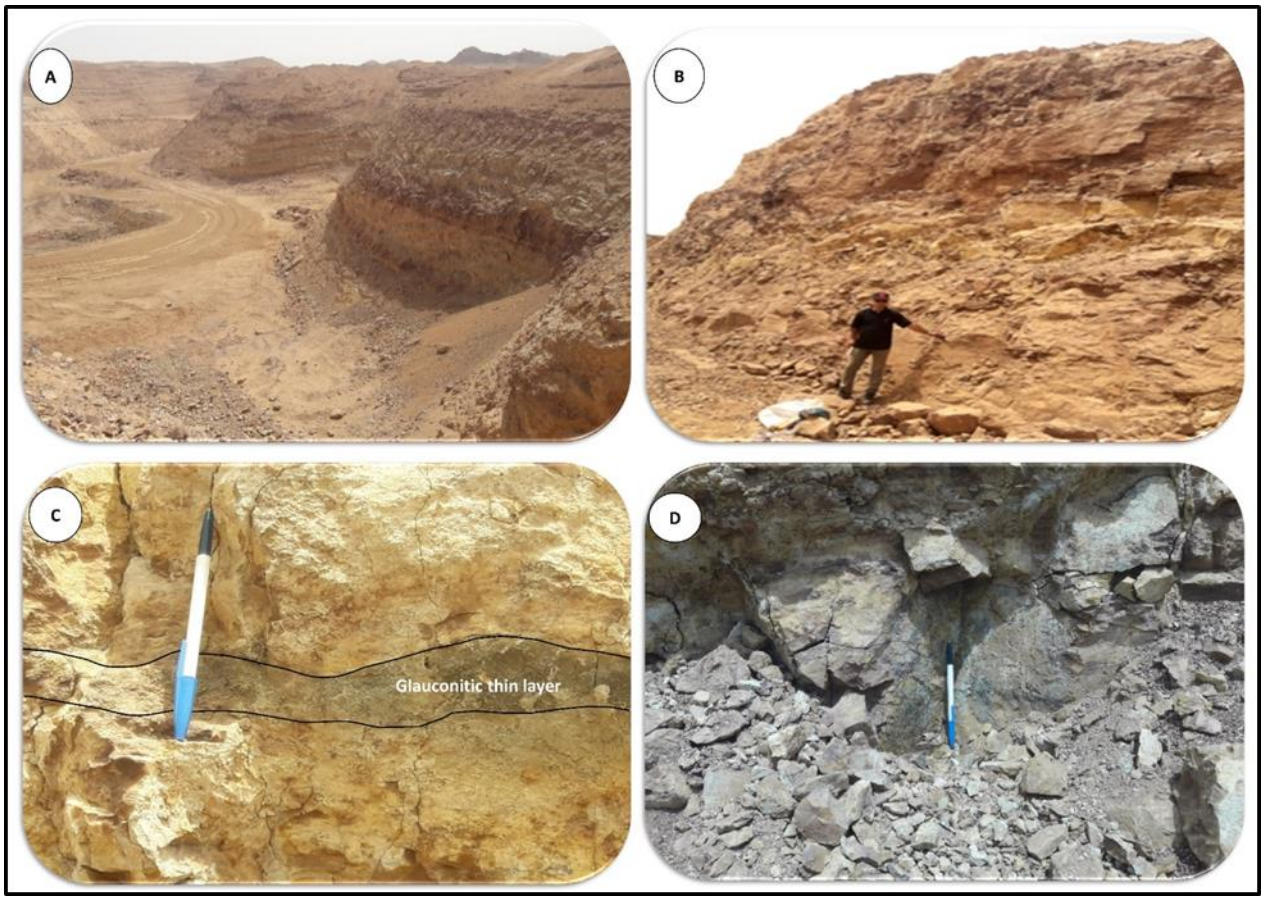

Fig. 3. Field photographs showing (A) open cast mining of kaolin mineral in the Abu Darag section, (B) ferruginous kaolinitic clay at the Wadi Araba section, (C) lenses of intercalated glauconitic bed in the Wadi Araba section, (D) surficial weathering of kaolinitic clay at Wadi Araba section.

Al_2O_3 has a significant negative relationship with SiO2 (r= -0.83; Fig. 5a; Table 3), but a positively significant correlation with LOI and TiO2 oxide. Contrarily, SiO2 exhibits a substantial negative association (r=-0.89, -0.60, and -0.83, respectively) with LOI, Fe_2O_3, and TiO_2 oxides, while, SiO_2 exhibits a substantial negative association (r= -0.89, -0.60, and -0.83, respectively) with LOI, Fe_2O_3, and TiO_2 oxides (Fig. 5d, e, and f; Table 3). Ca, Na, and K contents in the investigated samples were low, with average concentrations of 0.17, 0.34, and 0.82, respectively (see Table 1). Al_2O_3/SiO_2 ratios and LOI show a high positive connection (r= 0.91; Fig. 5g).

The SiO_2/Al_2O_3 ratio for the tested clay samples varied between 1.74 and 7.51. (With a 2.64 average). On the other hand, the Al_2O_3/SiO_2 ratio varied from 0.13 to 0.58. With a variance of 0.42 (Table 1)

Strontium and barium depletion are present in all of the samples being examined. (with an average of 113 and 273 ppm, respectively) in Table (2). Additionally, Sr exhibits a negligibly low correlation with Al_2O_3 and SiO_2 (r= -0.11). Ba, on the other hand, has a weak correlation with SiO_2 (r=-0.21) and a weak correlation with Al_2O_3 (r= -0.23) Table (3). Zirconium is more abundant in the examined samples (with an average concentration of 258 ppm), and it correlates negatively with SiO_2 (r= -0.61) and favorably with Al_2O_3.

Geochemical parameters

According to Fig. 6a, which shows the examined samples represented on the (Al_2O_3-CaO*+Na_2O-K_2O) ternary graph, all of the samples are placed in the Al_2O_3 (100%) zone at the top of the (A-CN-K) diagram, demonstrating the prevalence of aluminous clay minerals in the samples. All of the analyzed kaolinitic clay samples were shown to be represented at the A top of the A-CNK-FM graph, which represents the kaolinite and gibbsite groups (Fig. 6b).

The analysis of the ternary ($5Al_2O_3$–SiO_2–2CaO) diagram reveals that the samples under investigation fall inside the clay mineral zone at the top of the Al_2O_3–SiO_2 border (Fig. 6c). However, the binary diagram plotting SiO_2 against Al_2O_3+Na_2O+K_2O reveals that all of the examined samples, except for three that are plotted within the semi-humid field, are plotted within the semi-arid field and exhibit only minor chemical weathering and maturation (Fig. 6d). The results reveal that all of the examined samples are displayed in the non-marine field using the relationship among K_2O/Al_2O_3 and MgO/Al_2O_3 (Fig. 6e). A bivariate chart showing the analyzed samples' zirconium against titanium oxide plot reveals that they range from felsic to intermediate igneous rocks (Fig. 6f). The observations of charting SiO_2 vs. log (K_2O/Na_2O) show that the majority of the analyzed kaolin samples are connected to the active and passive continental boundaries, with only two samples falling within the island arc field (Fig. 6g). The analyzed sample's predecessor rocks appear to be predominantly basalt with minor admixtures of rhyolite or granite, according to a plot of Al_2O_3 against TiO_2 (Fig. 6h). The results of the dispersed plot (Al_2O_3-SiO_2-Fe_2O_3) ternary diagram revealed that all of the samples examined belong to the kaolinite and bauxitic kaolinite areas (Fig. 6i). The samples' Al_2O_3/TiO_2 ratios, which are associated with felsic igneous rocks, ranged from 18.15 to 38.34 (with an average of 23.97; Table 1).

Paleo-weathering conditions

The structure of the parent bedrock, the period of erosion, the climate, and the rate of continental uplift at the source location all play a significant role in determining how much chemical weathering of the source rocks occurs (Wronkiewicz and Condie, 1987). Since Ca, Na and K are mostly depleted from source rocks during chemical reactions, the amount of these elements in sediments created from the rocks acted as a barometer for the weathering's intensity (Nesbitt, et al., 1997). In feldspar and recent source rocks, the typical CIA ratio is 50, which indicates early weathering. Because of the severe weather, the CIA is greater than 80. It can get as high as 100 in residual weathering products like kaolinite and gibbsite. Low CIA levels, however, are due to cold, arid circumstances, which result in fewer chemical alterations. CIA is a weathering range of 60 to 80. The molecular ratios in the following equation can be used to get this index:

$$CIA = [Al_2O_3/ (Al_2O_3+CaO^*+Na_2O+K_2O)] *100 \quad \text{(Eq. 1)}$$

In this work, the CIA values are close to 100, as shown in Table 1. The CIA results of each sample under examination range between 77.75 and 99.34. (with an average of 94.60). The analyzed samples' CIW index values are greater than CIA values due to the absence of K_2O from the index (Table 1). The following examples demonstrate how to compute source area weathering and elemental redistribution during diagenesis using the alteration's plagioclase index:

$$PIA = [(Al_2O_3-K_2O) / (Al_2O_3+CaO^*+Na_2O-K_2O)] *100 \quad \text{(Eq. 2)}$$

Reduced PIA values (less than 50) are associated with unweathered or fresh rock samples, whereas high PIA values (> 84) would imply a significant intensity of chemical weathering. In all the examined samples,' PIA values range from 78.28 to 99.93. (with an average of 98.03; Table 1). According to CIA and PIA values, the investigated kaolin deposits show a high degree of chemical weathering.

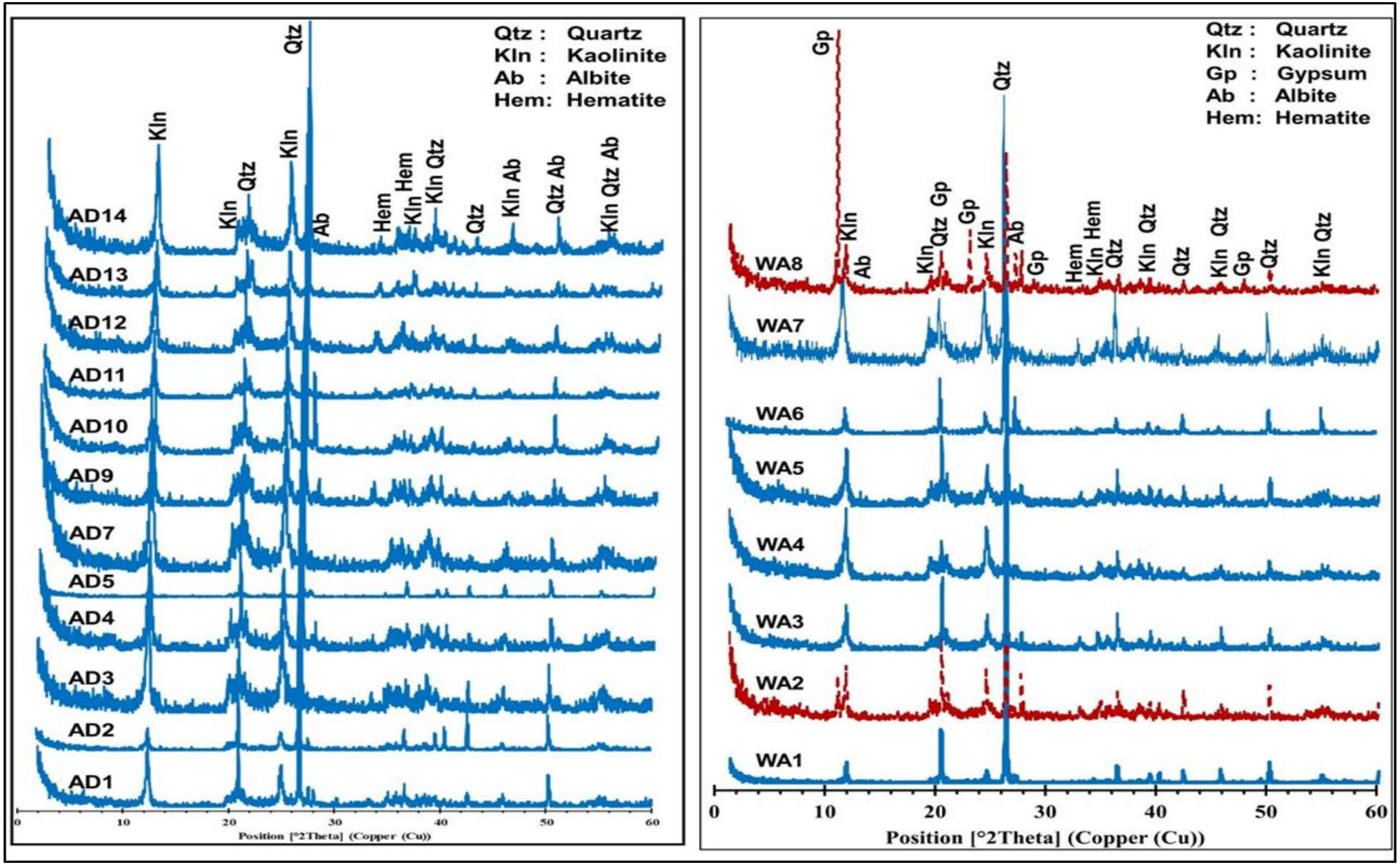

Fig. 4. XRD pattern of the studied samples at the Abu Darag and Wadi Araba sections in the Abu Darag area. Note the mineral abbreviations for rock-forming minerals taken from Kretz (1983); Whitney and Evans (2010).

Table 1. Whole-rock geochemical compositions of the studied kaolin samples (major oxides % and trace elements ppm) with some geochemical ratios

Samples	AD 1	AD 2	AD 3	AD 4	AD 5	AD 7	AD 9	AD 10	AD 11	AD 12	AD 13	AD 14	WA 1/1	WA 1/2	WA 1/3	WA 1/4	WA 1/5	WA 1/6	WA 2/1	WA 2/2	WA 2/3	WA 2/4	WA 2/5	WA 2/6	WA 2/7	WA 2/8
SiO_2	56.5	77.2	54.3	54.1	83.5	51.9	51.4	57.9	50.9	51.9	46.3	52.4	54.1	57.9	53.4	58.6	57.6	56.9	65.6	55.8	55.8	54.9	56.5	67.1	53.2	52.8
TiO_2	1.11	0.50	1.04	1.13	0.29	1.27	1.19	1.31	1.21	1.06	0.90	1.04	1.02	1.04	1.06	1.02	1.16	1.24	0.67	1.13	1.07	1.03	1.09	0.63	1.09	1.03
Al_2O_3	24.5	14.9	26.5	25.6	11.1	29.9	27.1	29.1	25.5	24.6	21.4	28.4	25.2	23.5	25.3	21.0	22.3	22.5	19.2	23.1	23.6	26.9	23.8	16.3	27.5	22.3
Fe_2O_3	8.55	3.06	6.90	9.01	2.67	5.50	8.70	1.37	12.2	11.8	15.2	5.90	9.31	8.59	10.5	10.3	10.4	10.2	7.30	9.57	10.8	6.30	8.94	8.16	7.33	8.23
MnO	0.01	0.01	0.01	0.01	0.01	0.01	0.01	0.01	0.01	0.01	0.01	0.01	0.01	0.01	0.01	0.01	0.01	0.01	0.01	0.01	0.01	0.01	0.01	0.01	0.01	0.01
MgO	0.49	0.01	0.25	0.08	0.01	0.01	0.08	0.06	0.08	0.20	0.01	0.05	0.89	0.95	0.58	0.98	0.92	0.97	1.22	0.88	0.70	0.75	0.79	0.97	0.45	1.23
CaO	0.01	0.01	0.01	0.01	0.01	0.01	0.01	0.01	0.01	0.01	0.01	0.01	0.01	0.01	0.01	0.01	0.01	0.17	0.01	0.43	0.01	0.01	0.01	0.01	0.01	3.66
Na_2O	0.01	0.01	0.01	0.01	0.01	0.01	0.01	0.01	0.01	0.66	5.86	1.45	0.01	0.01	0.01	0.01	0.20	0.36	0.01	0.01	0.01	0.01	0.01	0.01	0.01	0.03
K_2O	0.73	0.72	0.54	0.67	0.64	0.18	0.55	0.97	0.83	0.69	0.26	0.29	0.91	1.07	0.68	0.95	1.08	1.02	1.69	1.11	1.01	1.01	1.08	1.14	0.60	0.99
P_2O_5	0.01	0.01	0.01	0.02	0.01	0.01	0.01	0.01	0.01	0.01	0.01	0.01	0.01	0.01	0.01	0.01	0.01	0.16	0.01	0.01	0.01	0.01	0.01	0.01	0.01	0.01
Cl	0.01	0.01	0.01	0.01	0.01	0.01	0.01	0.01	0.01	0.03	0.10	0.04	0.01	0.01	0.01	0.01	0.01	0.01	0.01	0.01	0.01	0.01	0.01	0.01	0.01	0.01
SO_3	0.03	0.01	0.01	0.01	0.02	0.01	0.01	0.01	0.03	0.01	0.01	0.01	0.01	0.02	0.01	0.03	0.02	0.04	0.03	0.13	0.01	0.01	0.01	0.09	0.03	0.89
LOI	7.78	3.28	10.2	9.16	1.49	10.9	10.6	9.14	8.91	8.75	9.63	10.2	8.20	6.64	8.11	6.80	6.01	6.11	4.05	7.63	6.82	8.86	7.53	5.25	9.50	8.55
Total	99.8	99.8	99.8	99.7	99.8	99.8	99.7	99.9	99.8	99.7	99.7	99.8	99.7	99.8	99.8	99.7	99.8	99.7	99.8	99.7	99.8	99.7	99.7	99.7	99.7	99.7
V	158	47	163	186	34	179	132	154	217	181	251	140	225	168	177	163	178	163	89	167	172	184	169	87	188	159
Cr	144	41	132	107	333	189	119	117	107	111	114	116	127	114	139	138	135	127	79	124	126	139	126	130	157	120
Zn	66	15	45	45	22	31	49	35	50	58	60	38	70	60	49	81	64	68	94	72	69	66	70	84	47	61
Co	33	36	26	35	29	19	33	1	42	42	55	19	38	31	37	41	39	35	29	37	38	23	42	35	29	34
Sr	109	25	55	63	19	35	50	61	62	56	50	47	98	94	76	122	85	165	67	213	79	83	63	250	56	856
Zr	279	146	298	365	83	246	391	472	478	252	330	378	210	185	197	175	210	213	148	255	221	262	215	183	227	286
Ba	315	121	223	234	79	293	220	317	245	335	157	200	250	742	206	326	291	310	299	268	271	289	270	310	261	263
CIA	97.1	95.3	97.9	97.4	94.4	99.3	97.9	96.7	96.8	94.8	77.8	94.2	96.4	95.6	97.3	95.6	94.5	93.6	91.8	93.7	95.8	96.3	95.9	93.4	97.8	82.7
ICV	0.40	0.26	0.29	0.38	0.30	0.19	0.35	0.08	0.52	0.55	1.00	0.27	0.44	0.45	0.47	0.58	0.57	0.57	0.53	0.52	0.53	0.30	0.46	0.63	0.31	0.63
CIW	99.9	99.8	99.9	99.9	99.8	99.9	99.9	99.9	99.9	97.3	78.5	95.1	99.9	99.9	99.9	99.9	99.1	97.7	99.9	98.1	99.9	99.9	99.9	99.8	99.9	85.8
PIA	99.9	99.8	99.9	99.9	99.8	99.9	99.9	99.9	99.9	97.3	78.3	95.1	99.9	99.9	99.9	99.9	99.0	97.6	99.8	98.0	99.9	99.9	99.9	99.8	99.9	85.3
V/Cr	1.10	1.15	1.23	1.74	0.10	0.95	1.11	1.32	2.03	1.63	2.20	1.21	1.77	1.47	1.27	1.18	1.32	1.28	1.13	1.35	1.37	1.32	1.34	0.67	1.20	1.33
SiO_2/Al_2O_3	2.30	5.16	2.05	2.11	7.51	1.74	1.90	1.99	2.00	2.11	2.16	1.85	2.15	2.46	2.11	2.79	2.58	2.53	3.43	2.42	2.37	2.04	2.37	4.11	1.93	2.37
Al_2O_3/SiO_2	0.43	0.19	0.49	0.47	0.13	0.58	0.53	0.50	0.50	0.47	0.46	0.54	0.47	0.41	0.47	0.36	0.39	0.40	0.29	0.41	0.42	0.49	0.42	0.24	0.52	0.42
K_2O/Na_2O	73	72	54	67	64	18	55	97	83	1	0	0	91	107	68	95	5	3	169	111	101	101	108	114	60	33
K_2O/Al_2O_3	0.03	0.05	0.02	0.03	0.06	0.01	0.02	0.03	0.03	0.03	0.01	0.01	0.04	0.05	0.03	0.05	0.05	0.05	0.09	0.05	0.04	0.04	0.05	0.07	0.02	0.04
Al_2O_3/TiO_2	22.1	29.9	25.5	22.6	38.3	23.5	22.8	22.2	21.0	23.2	23.8	27.3	24.7	22.6	23.9	20.6	19.2	18.2	28.6	20.4	22.1	26.1	21.8	25.9	25.3	21.7
TiO_2/Al_2O_3	0.05	0.03	0.04	0.04	0.03	0.04	0.04	0.05	0.05	0.04	0.04	0.04	0.04	0.04	0.04	0.05	0.05	0.06	0.03	0.05	0.05	0.04	0.05	0.04	0.04	0.05
MgO/Al_2O_3	0.02	0.00	0.01	0.00	0.00	000	0.00	0.00	0.00	0.01	0.00	0.00	0.04	0.04	0.02	0.05	0.04	0.04	0.06	0.04	0.03	0.03	0.03	0.06	0.02	0.06

* Note: AD = Abu Darag section and WA = Wadi Araba section

Table 2. Average major oxides (wt. %) and trace elements (ppm) in the studied samples compared with other international works

Oxides	SiO_2	TiO_2	Al_2O_3	Fe_2O_3	MnO	MgO	CaO	Na_2O	K_2O	LOI	V	Cr	Zn	Sr	Zr	Ba
Pettijohn (1957)	58.10	0.60	15.40	4.02	Na	2.40	3.10	1.30	3.24	Na	Na	Na	Na	Na	Na	Na
Turekian and Wedepohl (1961)	58.50	0.77	15.00	6.7	Na	2.50	3.10	3.10	1.2	Na	130	90	95	300	160	580
Wedepohl (1978)	Na	0.9	16.7	4.8	Na	3.3	3.3	0.6	6.8	12.1	110	14	100	359	167	360
NASC – Gromet, et al. (1984)	64.82	0.80	17.05	5.70	Na	2.83	3.51	1.13	3.97	Na	130	125	Na	142	200	636
PAAS - Taylor and McLennan (1985)	62.40	0.99	18.78	7.18	Na	2.19	1.29	1.19	3.68	Na	150	Na	85	200	210	650
Condie (1993)	63.6	0.82	17.8	5.89	Na	2.3	1.3	1.1	3.84	Na	117	Na	Na	136	201	551
Montes, et al. (2002)	41.58	1.69	37.35	4.37	Na	0.01	0.02	0.02	0.01	15.23	Na	Na	Na	Na	Na	Na
Wilson (2004)	44	0.27	38.13	0.37	Na	0.23	0.45	0.31	0.30	16.13	Na	Na	Na	Na	Na	Na
Sayin (2007)	64.7	0.30	24.74	0.66	0.10	0.09	0.06	0.22	0.76	8.14	78.3	308	26.33	1464	308	664
Baioumy and Gilg (2011)	48.20	2.8	35	1.26	0.01	0.24	0.07	0.14	0.03	12.60	415	435	68	38	1296	66
Baioumy, et al. (2012)	58.63	1.77	21.51	4.92	0.04	0.6	0.09	0.7	0.9	10.20	176	Na	12.4	177	246	159
Okunlola and Idowu (2012)	61.26	1.74	16.55	3.75	Na	0.16	0.05	0.06	1.39	Na	109	Na	116.4	59.39	1157	394
Grecco, et al. (2012)	74	0.16	18.33	0.13	0.01	0.12	0.11	0.05	0.04	6.95	37.4	20	30	795	101	1239
Khater, et al. (2013)	49.86	0.88	34.10	0.30	0.01	0.26	0.09	0.03	0.02	13.44	Na	Na	Na	Na	Na	Na
El-Kammar, et al. (2017)	56.29	2.08	28.16	2.05	Na	0.16	0.27	0.13	0.42	10.07	189	Na	Na	144	Na	Na
Saber, et al. (2018)	40.95	3.24	36.08	5.34	Na	0.91	0.12	0.33	0.04	Na	360	109	Na	66.10	1206	28.62
El Nagar and Khater (2019)	49.86	0.88	34.10	0.30	0.01	0.26	0.09	0.03	0.02	13.44	Na	Na	Na	Na	Na	Na
Khater and El Nagar (2019)	56.33	3.73	27.61	1.32	Na	0.06	0.18	0.08	0.04	10.17	Na	Na	Na	Na	Na	Na
Present work (2022)	57.24	1.01	23.51	8.34	0.01	0.52	0.17	0.34	0.82	7.70	159	131	57	113	258	273

*Note: Na related to not analyzed

Table 3. Pearson correlation coefficient matrix for the major oxides and trace elements in the studied clay samples.

	SiO_2	**TiO_2**	**Al_2O_3**	**Fe_2O_3**	**MnO**	**MgO**	**CaO**	**Na_2O**	**K_2O**	**P_2O_5**	**Cl**	**SO3**	**LOI**	**V**	**Cr**	**Zn**	**Co**	**Sr**	**Zr**	**Ba**
SiO_2	1.00																			
TiO_2	-0.83	1.00																		
Al_2O_3	-0.83	0.88	1.00																	
Fe_2O_3	-0.60	0.32	0.10	1.00																
MnO	0.00	0.00	0.00	0.00	1.00															
MgO	0.02	0.01	-0.19	0.24	0.00	1.00														
CaO	-0.12	0.03	-0.06	0.01	0.00	0.36	1.00													
Na_2O	-0.32	-0.07	-0.04	0.45	0.00	-0.29	-0.06	1.00												
K_2O	0.29	-0.13	-0.32	0.01	0.00	0.79	0.13	-0.42	1.00											
P_2O_5	-0.01	0.20	-0.04	0.13	0.00	0.20	0.00	0.00	0.12	1.00										
Cl	-0.33	-0.08	-0.01	0.44	0.00	-0.34	-0.07	0.99	-0.46	-0.06	1.00									
SO3	-0.09	0.00	-0.10	0.02	0.00	0.39	1.00	-0.06	0.16	-0.02	-0.07	1.00								
LOI	-0.89	0.77	0.90	0.25	0.00	-0.31	0.07	0.22	-0.53	-0.13	0.25	0.04	1.00							
V	-0.89	0.73	0.67	0.67	0.00	0.02	0.00	0.37	-0.22	0.02	0.36	-0.02	0.71	1.00						
Cr	0.34	-0.27	-0.24	-0.27	0.00	-0.17	-0.05	-0.10	-0.26	-0.02	-0.11	-0.05	-0.22	-0.22	1.00					
Zn	-0.23	0.11	-0.07	0.54	0.00	0.81	0.07	0.00	0.69	0.12	-0.02	0.12	-0.10	0.24	-0.27	1.00				
Co	-0.12	-0.17	-0.38	0.81	0.00	0.20	0.03	0.39	0.04	0.04	0.37	0.04	-0.17	0.28	-0.16	0.38	1.00			
Sr	-0.11	0.03	-0.11	0.08	0.00	0.52	0.96	-0.10	0.26	0.06	-0.12	0.98	0.02	0.00	-0.09	0.26	0.07	1.00		
Zr	-0.61	0.62	0.66	0.10	0.00	-0.47	0.05	0.20	-0.33	-0.08	0.22	0.04	0.73	0.46	-0.30	-0.22	-0.27	0.00	1.00	
Ba	-0.21	0.34	0.23	0.13	0.00	0.45	-0.02	-0.22	0.38	0.06	-0.21	0.00	0.07	0.21	-0.21	0.38	-0.12	0.08	-0.06	1.00

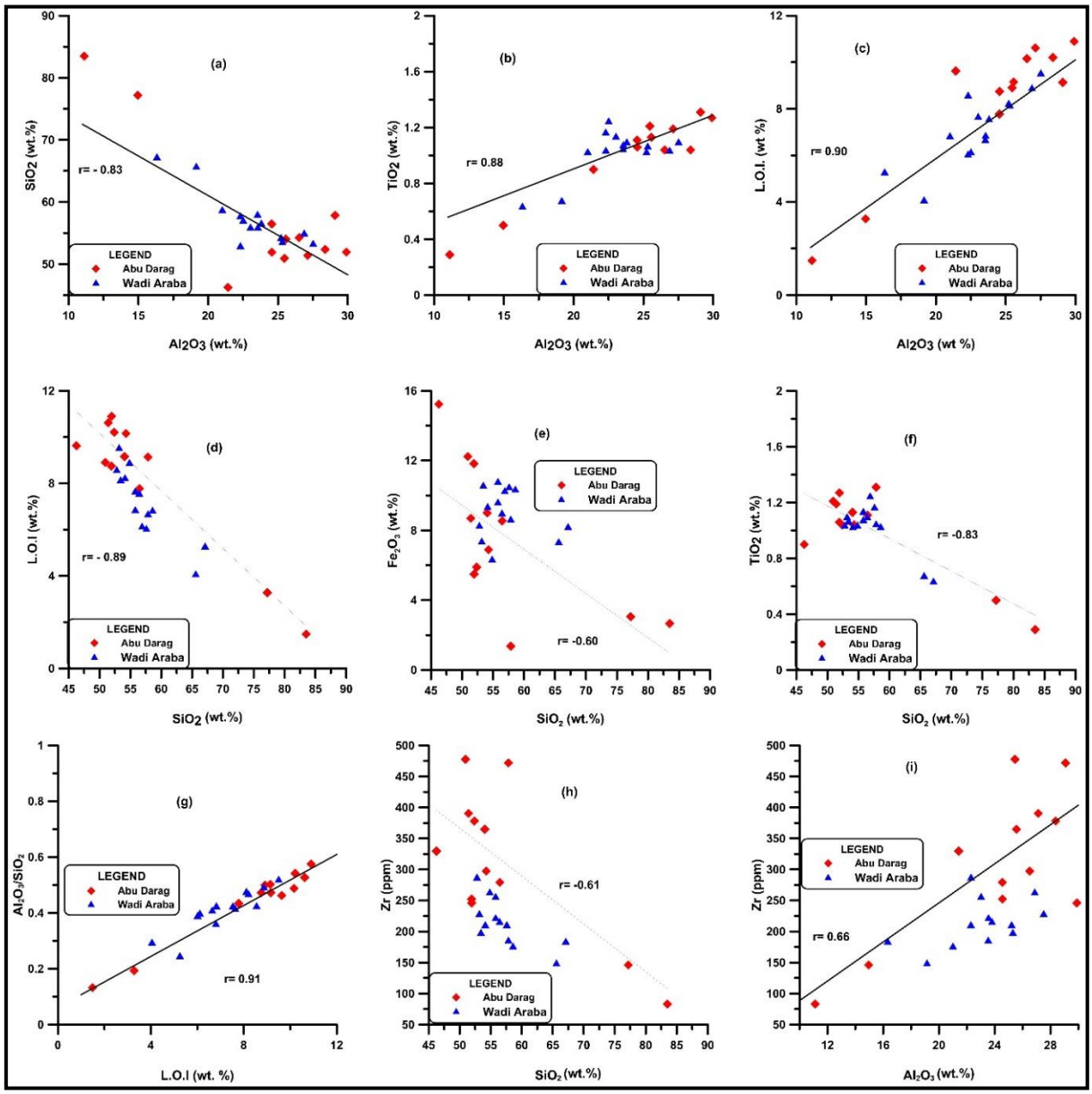

Fig. 5. Inter-elemental relationships between major oxides (wt. %) and trace elements (ppm) of the analyzed kaolin samples.

Whole-rock geochemistry

The examined kaolin samples' geochemical analysis revealed significant concentrations of SiO2 and Al_2O_3, which indicated poor kaolinite and high quartz contents (Table 1). Quartz and kaolinite were the two main elements of the investigated kaolin samples that the XRD analysis was able to identify. These samples contain detrital quartz grains that are made up of different materials. According to geochemical data, there isn't much Al_2O_3 in the area. This is indicated by a strong negative correlation between Al_2O_3 and SiO2 (r = -0.83), which is an indication of the

little impact that feldspar weathering, dissolution, and partial silica migration have under high pH environmental conditions.

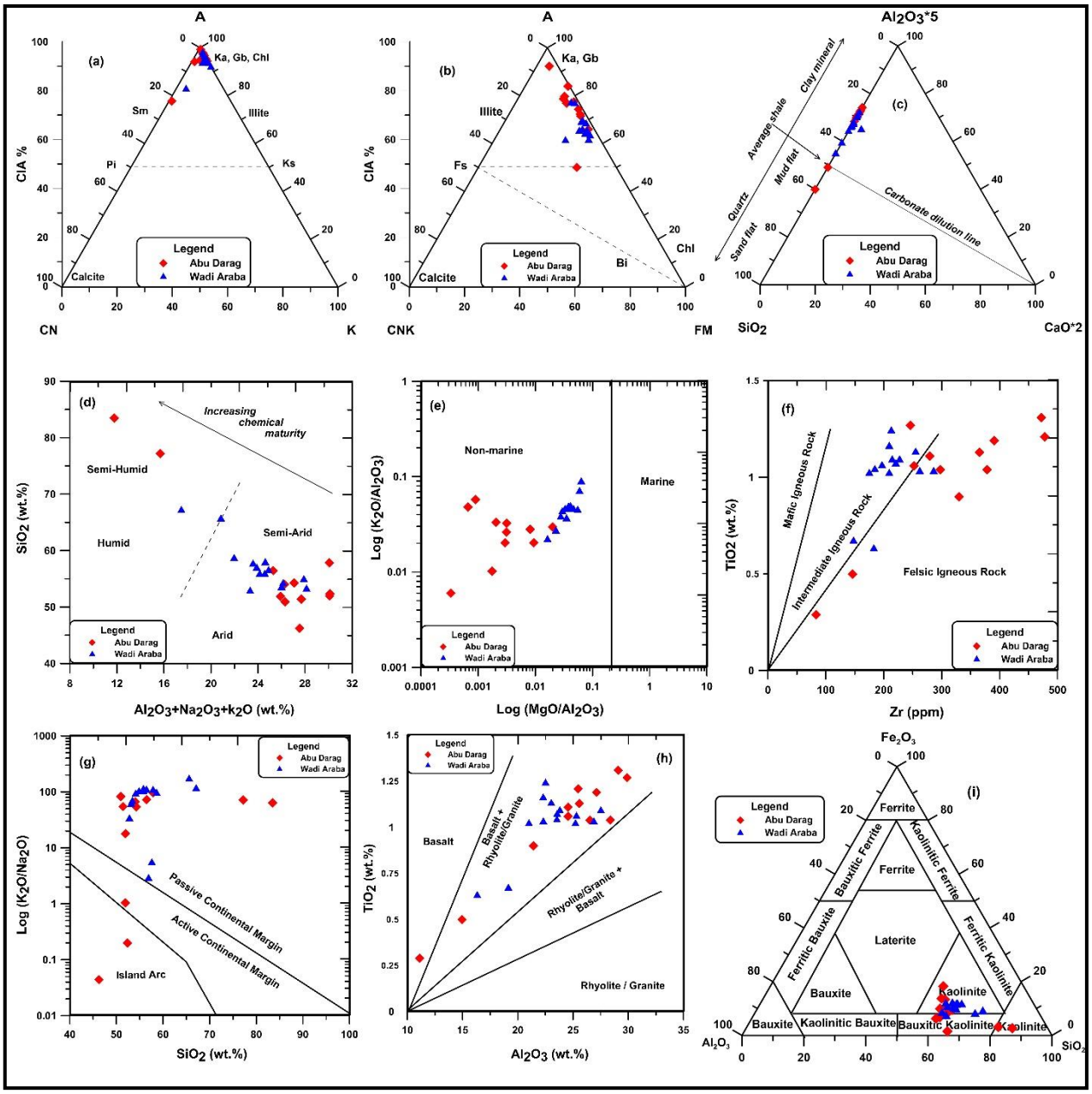

Fig. 6. (a and b) A-CN-K and A-CNK-FM ternary diagrams (Ka= kaolinite, Gb= gibbsite, Chl= chlorite, Sm= smectite, Pl= plagioclase, Ks= K-feldspar, Fs=feldspar, Bi=biotite, A=Al_2O_3, CN= CaO*+Na_2O_3, CNK= CaO*+Na_2O_3+K_2O, and FM= FeO*+MgO (after Nesbitt, et al., 1984 and 1989). (c) $5Al_2O_3$ - 2CaO - SiO_2 ternary diagram (after Brumsack, 1989). (d) Bivariate plot diagrams (Al_2O_3+ Na_2O+K_2O) against SiO_2 (after Suttner and Dutta 1986). (e) the scattered plot of log (Mg/Al) against (K/Al) (after Roaldest, 1978). (f) Plotted Zr vs. Ti (after Hayashi, et al., 1977). (g) plotted SiO_2 vs. K_2O/Na_2O (after Roser and Korsch, 1986). (h) Al_2O_3 against TiO_2 (after Hayashi, et al., 1977). (i) $Fe_2O_3/Al_2O_3/SiO_2$ (after Aleva, 1994).

Plagioclase, quartz, and clay minerals can all be found together, which suggests a connection between the two. On the other hand, the Al_2O_3 content of shale may be connected to the preferred assimilation of aluminous clays (Al-Juboury, et al., 2021). Neutral weathering begins with the complete dissolution of feldspars in an ionic solution. In contrast to silica, which cannot be removed from the acid solution (pH 4), aluminum may be precipitated from it with a high degree of purity (Rankama and Sahama, 1950; Goldschmidt, 1954; Cox, 1995). Not linked, demonstrating that clay minerals have no impact on detrital silicates, the predominant type of SiO_2 (Wang, et al., 2017). The ability of Al to be substituted by Fe and Ti ions may be connected to the presence of TiO2 and Fe2O3 in the samples under investigation. Fe is found in the form of Fe-oxides, and Ti is found as anatase, according to XRF and XRD measurements (Fig. 4 and Table 1). Due to their isolated nature and lack of involvement in the development of the kaolinite structure, Ti and Fe appear to be distributed randomly. Due to their isolated nature and lack of involvement in the development of the kaolinite structure, Ti and Fe appear to be distributed randomly. On the other hand, higher Fe_2O_3 content is linked to more basic ancestors, while higher Ti concentration is linked to younger Neogene basaltic dykes.

Kaolin clays derived from mafic parent materials often contain high TiO_2 concentrations because weathering significantly removes silica and alkali ions. The Fe and Ti oxides may be slightly related to the fine grains fraction or may exist in distinct later phases, according to the positive relationship between Al_2O_3 and the two oxides. Because Si is present but Fe and Ti are not, these elements may be coated on quartz grains (Masoud, et al., 2013). The strong negative connection of L.O.I vs. SiO_2 and the large positive correlation of L.O.I toward Al_2O_3 indicate that clay minerals are the main source of L.O.I. Al/Si ratios also show a substantial positive correlation with the L.O.I value, indicating that they might be used as a kaolin quality indicator. Al/Si ratio is still less than the value of 0.85 even if it is lower than the value of 0.85 that was assigned to flawless kaolin (Schroeder, et al., 2004; Ga'miz, et al., 2005).

The low concentration of alkali elements (such as Ca, Na, and K), Sr, and Ba in the study samples is indicative of the depletion of these elements. This may be because some feldspar crystals have not yet undergone the transformation into clay minerals, and these elements have high mobility (McLennan, et al., 1983; Saber, et al., 2018). The examined materials' SiO_2/Al_2O_3 ratio (2.64) (Table 1) is nearly identical to that of pure montmorillonite (Felix, 1977). He claimed that although pure montmorillonite has a range of 2.80 to 3.31, pure kaolinite has a Si/Al ratio of approximately 1.18. The chemical maturities of the examined samples range from dry to semi-arid climatic zones and barely reflect chemical weathering and maturity. Different levels of weathering and climatic change in the studied samples could be the reason for the scattering of the displayed samples. The A/CN/K plot indicates an intermediate weathering history with gabbros, tonalities, and granodiorite trends, but the A/CN/K plot defines a non-homogenous source between the weathering trends of basaltic and granitic rocks and is moderately influenced by chemical weathering (Alqahtani and Khalil, 2021). The Early Cretaceous (Aptian-Albian) era of the research area, which is a region of Northeast Africa, saw a progressive change in the paleoclimate from tropical to desert, as evidenced by the paleoclimatic maps from Chumakov (1995), which are displayed in Hay and Floegel (2012) and those from Boucot, et al (2013). According to the examined samples from the non-marine field, the studied materials were either deposited under oxidation or supergene continental conditions. Clays having a high TiO_2/Al_2O_3 ratio, according to Migdisove (1960), are a symptom of a humid climate.

This ratio ranged from 0.03 to 0.06 (with an average of 0.04) for the examined samples, indicating an arid climate, which is in line with the fact that Ti is of terrigenous origin and largely related to clay minerals. TiO_2 is generally found distributed throughout clays as separate minerals, which include rutile and anatase since Ti can replace Al (Degens, 1965), or be mixed into kaolinite (Dai, et al., 2015). An XRD examination of the investigated materials revealed the accessory mineral anatase (Fig. 4). Older sediments' K_2O/Al_2O_3 ratios can be used to ascertain their original composition. K_2O/Al_2O_3 ratios in clay minerals and feldspars vary (0.0 to 0.3 and from 0.3 to 0.9, respectively; Cox, et al., 1995). The average K_2O/Al_2O_3 ratios of the studied samples range from 0.01 to 0.09 and are consistent with clay minerals (with an average of 0.04; Table 1).

Various authors have utilized the V/Cr ratio as a sign of paleo-oxygenation. Anoxic depositional circumstances are assumed to be represented by V/Cr values > 2, whilst more oxidizing conditions are thought to be represented by V/Cr values 2. (Dill, et al., 1988) The studied kaolin samples have a V/Cr value that ranges from 0.10 to 2.20 (with an average of 1.30), which suggests that these sediments were generated under more oxidizing circumstances, as seen by the high vanadium and low chromium values. The high vanadium values are explained by the fact that clay minerals are generated when igneous rocks weather and that some vanadium in marine hydrolysate deposits may be bound in clay minerals (Goldschmidt, 1954).

The relatively limited mobility during sedimentary processes, trace elements like La, Y, Sc, Cr, Th, Zr, Hf, Nb, and especially TiO2 among other significant elements are best suited for provenance and tectonic setting determination studies (McLennan, et al., 1983). Moreover, by comparing the relative distribution of immobile elements with different concentrations in felsic and basic igneous rocks, such as La and Th (enriched in the felsic igneous rocks) and Sc, Cr, and Co (infused in the basic igneous rocks relative to the felsic igneous rocks), it has been possible to determine the relative contributions of felsic and basic sources in shales from different tectonic environments (Wronkiewicz and Condie, 1987).

The source rock for the samples under study was predominately basalt, with minor admixtures of rhyolite and granite. High rainfall, gentle slopes, a fluctuating water table, and quick water percolation caused these source rocks to condition and change quickly into kaolinite and quartz minerals (Murray and Keller, 1993). The analyzed samples' Al_2O_3/TiO_2 ratio is greater than 21, which points to the source rocks' felsic igneous origin. The high and/or extreme chemical weathering of their sources is reflected in the CIA readings, which have an average of 94.60. The high CIA values of the examined kaolin samples reveal the elimination of extremely immobile or stable residual constituents (such as Al and Ti) relative to mobile or unstable cations (such as Ca, Na, and K) during weathering (Nesbitt and Young, 1982; Hiroaki and Bah Mamadou, 2016).

The PIA index demonstrates that during source weathering, transport, sedimentation, and diagenesis, feldspars were chemically worn and damaged significantly. Fedo, et al. (1995) refer to the high PIA values found in plagioclase, which is significantly chemically weathered. During the initial stages of weathering, Ca is leached more quickly than Na and K. With an increase in the K/Na ratio (K_2O/Na_2O), the overall alkali content ($K_2O + Na_2O$), which decreases with more weathering, increases. This is because plagioclase is being eliminated more effectively than K-feldspars while feldspars are being destroyed (Nesbitt and Young, 1984). The individual graphs of K/Na, K+Na, Na, K, and Ca against PIA, according to Christopher, et al. (2017), show the mobility of elements during the last stage of chemical weathering of altered feldspars. The

bivariate graphs of Ca, Na, and K against PIA display the behavior of alkali elements during the chemical weathering of feldspars in the studied samples (Fig. 7a).

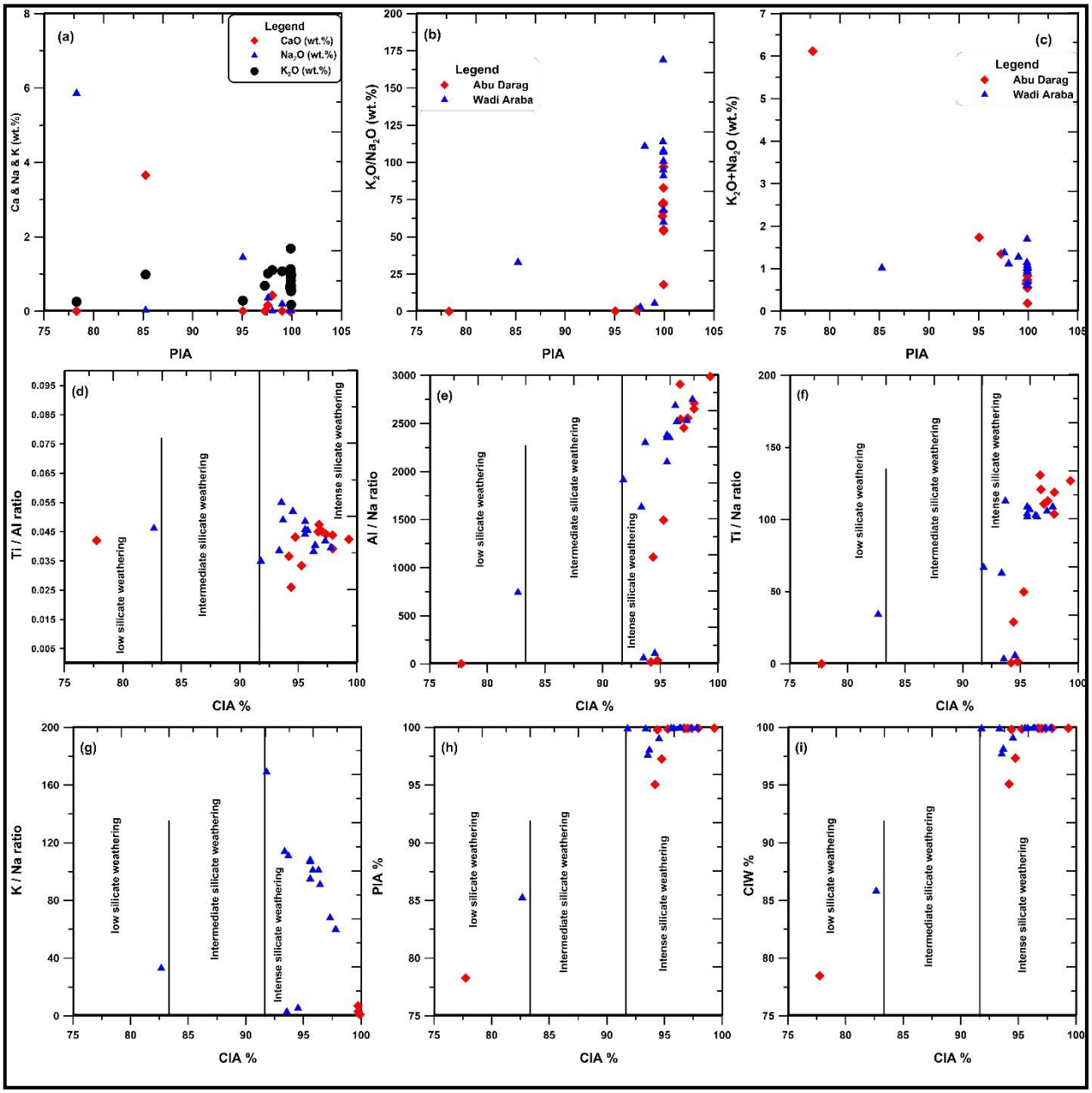

Fig. 7. (a) Relationship between PIA against Ca, Na, and K, (b) Bivariate plotted diagrams between PIA vs. K_2O/Na_2O, (c) Plotted diagrams between PIA against K_2O+Na_2O, (d) Binary plot of CIA vs. Ti/Al diagram, (e) CIA against Al/Na, (f) Scatter plots bivariate diagram of CIA vs. Ti/Na, (g) CIA vs. K/Na, (h) CIA against PIA, (I) CIA vs. CIW for the studied samples (after Christopher, et al., 2017).

Consequently, a plot of K/Na vs. PIA (Fig. 7b) showed that the K/Na levels in the examined samples frequently increase with a high value of PIA, whereas a plot of K+Na against

PIA reveals that, in the majority of the samples, the total content of alkalis declines with increasing PIA values. (Fig. 7c). The relationship between alkali elements (Ca, Na, and K) and PIA revealed an occurrence of highly anomalous in some samples. These findings show that the examined samples contained trace levels of albite and gypsum minerals, which were detected by XRD (Fig. 4).

The index of chemical weathering (CIA) has been linked to the elemental ratios Ti/Al, Al/Na, Ti/Na, K/Na, PIA, and CIW, according to Schneider, et al., 1997; Roy, et al., 2008; and Perri, 2014 (Fig. 7d to 7i). These ratios are used as indications of the intensity of chemical weathering. There are three categories for chemical weathering intensity: (no silicate weathering, low silicate weathering, intermediate silicate weathering, and intense silicate weathering). The relationship between the CIA and the Ti/Al, Al/Na, Ti/Na, and K/Na ratios shows that the degree of weathering has increased from low to primarily intense (Fig. 7d-g). Additionally, CIA values have more intense weathering compared to PIA and CIW values (Fig. 7h-i). CIA values of the studied samples don't show any linear relationship concerning elemental ratios. The intensity of source area weathering can be roughly estimated using these elemental ratios.

Conclusions

The current study allows for summarizing the following conclusions: The study area has a large reserve of kaolin deposits-roughly 54 million metric tons. It is thought that the source rocks of these kaolin deposits are the Precambrian basement rocks discovered in the vicinity of the research area, which were transported beyond the sedimentary basin to the north. Additionally, non-marine (fluvial) depositional settings are considered to be depositional environments. It shows that the materials under study where were left close to the Red Sea's coastal plain and experienced weak to moderate chemical weathering as well as severe physical induration, largely in non-marine environments.

The chemical markers of alteration reflect the substantial weathering of the parent rocks (CIA). With fluctuating water tables and ready water percolation, these weathering conditions point to a somewhat warm and humid palaeoclimate. Interestingly, the associations between the average CIA values and the average Al_2O_3 content were strongly negative. This pattern suggests that the Al_2O_3 composition was influenced not just by weathering intensity but also by input from several source rocks. According to geochemical data for main oxides and trace elements as well as bivariate discriminating provenance diagrams, the Malha Formation clastic deposits were primarily produced from felsic and intermediate igneous rocks, with a possible contribution from quartz-rich crystalline provenance.

Acknowledgments

The editorial staff of INJES, particularly the Editor-in-Chief, is gratefully acknowledged by the authors (Prof. Dr. Rayan Ghazi Thannoun). Special gratitude is given to all reviewers for their insightful criticism and suggestions, particularly Prof. Dr. Raghid Sabri, whose review helped to improve the entire work. The Egyptian Geological Survey (Central Laboratory Sector) received thanks from the authors for helping to provide the chemical analyses required for this study.

Conflict of Interest

The authors declare that there are no conflicts of interest regarding the publication of this manuscript.

References

Abdallah, A.m., and Adindani, A., 1963. Stratigraphy of Upper Paleozoic rocks, western side of the Gulf of Suez, Egypt. Egyptian Geological Survey, v. 25, 18 P.

Aleva, G.J.J., 1994. Laterites: Concepts, Geology, Morphology, and Chemistry. ISRIC, Wageningen, the Netherlands, 169 P.

Al-Juboury, A.I., Hussain, S.H., and Al-Lhaebi1, S.H., 2021. Geochemistry and mineralogy of the Silurian Akkas Formation, Iraqi western desert: implications for palaeoweathering, provenance, and tectonic setting. Arabian Journal of Geosciences, 14: 760, 24 P.

Alqahtani, F., and Khalil M., 2021. Geochemical analysis for evaluating the paleoweathering, paleoclimate, and depositional environments of the siliciclastic Miocene-Pliocene sequence at Al-Rehaili area, Northern Jeddah, Saudi Arabia. Arabian Journal of Geosciences, 14: 239, 12 P.

Álvarez, J.O.I., 2005. Geochemical study of the Mesoproterozoic Belt-Purcell super-group, Western North America: Implications for provenance, weathering, and diagenesis. A Thesis Submitted to the College of Graduate Studies and Research in Partial Fulfillment of the Requirements for the Degree of Doctor of Philosophy in the Department of Earth Sciences University of Saskatchewan Saskatoon, 243 P.

Armient, P., Messiga, B., and Vannucci, R., 1998. Sand provenance from major and trace element analyses of bulk rock and sand grains. Terra Antarctica 5(3), pp. 589-599.

Baioumy, H., and Gilg, H.A., 2011. Pisolitic flint kaolin from Kalabsha, Egypt: A laterit-derived facies. Sedimentary Geology, 236(1-2), pp. 141-152.

Barbera, G., Mazzoleni, P., Critelli, S., Pappalardo, A., Lo-Giudice, A., and Cirrincione, R., 2006. Provenance of shales and sedimentary history of the Monte Soro Unit. Sicily Per Mineral, 75(2–3), pp. 313-330.

Boucot, A.J., Xu, C., Scotese, C.R., and Morley, R.J., 2013. Phanerozoic paleoclimate: an atlas of lithologic indicators of climate. SEPM Concepts in Sedimentology and Paleontology No. 11: Map Folio, SEPM (Society for Sedimentary Geology). Gary J. Nichols and Brian Ricketts, SEPM Publications Editors, Tulsa, Oklahoma, U.S.A.

Brumsack, H.J., 1989. Geochemistry of recent TOC-rich sediments from the Gulf of California and the Black Sea. Geol. Rundsch, 78(3), pp. 851-882.

Chang, L., Howie, R., and Zussman, J., 1996. Rock-forming minerals, (2nd ed.) Non-silicates, v. 5, pp. 40-73 and 189-218.

Christopher, B., Kuiwu L., and Oswald, G., 2017. Geochemistry of sandstones and shales from the Ecca Group, Karoo Supergroup, in the Eastern Cape Province of South Africa: Implications for provenance, weathering, and tectonic setting. Open Geosci., Vol. 9, pp.340-360.

Chumakov, N., 1995. The problem of the warm biosphere. Stratigr. Geol. Correl. 3, pp. 205-215.

Condie, K.C., 1993. Chemical composition and evolution of the upper continental crust contrasting results from surface samples and shales. Chem. Geol., v. 104, pp. 1-37.

Correia, S., Curto, K., Hotza, D., and Segadaes, A., 2005. Clays from southern Brazil: Physical, chemical and mineralogical characterization. Material Science Forum, 498, pp. 447-452.

Cox, R., Lowe, D.R., and Cullers, R.L., 1995. The influence of sediment recycling and basement composition on evolution of mudrock chemistry in the southwestern United States. Geochimica et Cosmochimica Acta, 59(14), pp. 2919-2940.

Dai, S., Liu, J., Ward, C.R., Hower, J.C., French, D., Jia, S., Hood, M.M., and Garrison, T.M., 2015. Mineralogical and geochemical compositions of late Permian coals and host rocks from the Guxu coalfield, Sichuan Province, China, with emphasis on enrichment of rare metals. International Journal of Coal Geology, v. 166, pp. 71-95.

Darwish, M., 1992. Facies developments of the Upper Paleozoic-Lower Cretaceous sequences in the Northern Galala Plateau and evidence for their hydrocarbon reservoir potentiality, northern Gulf of Suez, Egypt, Cairo Univ., Cairo, pp. 75-214.

Degens, E.T., 1965. Geochemistry of sediments: A brief survey. Prentice-hall Inc., New Jersey, 103(4), 369 P.

Dill, H., Bosse, H.R., Henning, K.H., and Fricke, A., 1997. Mineralogical and chemical variations in hypogene and supergene kaolin deposits in a mobile fold belt in the Central Andes of Northwestern Peru. Miner. Deposita, 32, pp. 149-163.

Dill, H., Teschner, M., and Wehner, H., 1988. Petrography, inorganic, and organic geochemistry of Lower Permian Carbonaceous fan sequences (Brandschiefer Series), Federal Republic of Germany: constraints to their paleogeography and assessment of their source rock potential. Chem. Geol., 67(1-3), pp. 307-325.

El Nagar, A.M., and Khater, H.M., 2019. Development of high thermal stability geopolymer composites enhanced by nano metakaolin. J. Build. Mater. Struct., Vol. 6, pp. 10-19.

Farouk, S., 2016. Paleocene stratigraphy in Egypt. J African Earth Sci., v. 113, pp. 126-152.

Fedo, C.M., Nesbitt, H.W., and Young, G.M., 1995. Unraveling the effects of potassium metasomatism in sedimentary rocks and paleosols, with implications for paleo-weathering conditions and provenance. Sedimentary Geology, 23, pp. 921-924.

Felix, N.S., 1977. Physico-chemical studies on bentonites with special reference to Fayoum Deposits: Ph.D. Thesis, Fac. of Sci., Cairo, Univ. Egypt.

Folk, R., 1980. Petrology of sedimentary rocks. Hemphill publishing company, Austin, Texas, 184 P.

Frondel, C., 1962. Dana's the system of mineralogy, (7th edition) Wiley publisher, Silica minerals, v. 3, 250 P.

Ga´miz, E., Melgosa, M., Sa´nchez-Maranˇo´n, M., Martı´n-Garcı´a, J.M., and Delgado, R., 2005. Relationships between chemico-mineralogical composition and color properties in selected natural and calcined Spanish kaolins. Applied Clay Science, 28, pp. 269-282.

Goldschmidt, V.M., 1954. Geochemistry. Oxford University Press, Amen House, London E.C.4. 166 P.

Grecco, L.E., Marfil, S.A., and Maiza, P.J., 2012. Mineralogy and geochemistry of hydrothermal kaolins from the Adelita mine, Patagonia (Argentina); relation to other mineralization in the area. Clay Min., Vol. 47, pp. 131-146.

Gromet, L.P., Dymek, R.F., Haskin, L.A., and Korotev, R.L., 1984. The "North American shale composite": Its compilation, major and trace element characteristics. Pergamon Press Ltd. U.S.A. Geochimica et Cosmochimica Acta, 48, pp. 2469-2482.

Hay, W.W., and Floegel, S., 2012. New thoughts about the Cretaceous climate and oceans. Earth Sci. Rev., 115 (4), pp. 262–272.

Hayashi, K., Fujisawa, H., Holland, H., and Ohmoto, H., 1977. Geochemistry of ~1.9 Ga sedimentary rocks from northeastern Labrador, Canada. Geochimica et Cosmochimica Acta, 61(19), pp. 4115-4137.

Hiroaki, I., and Bah Mamadou, L.M., 2016. Geochemical classification and determination of maturity source weathering in beach sands of eastern San' in Coast, Tango Peninsula, and Wakasa Bay, Japan. Earth Science Research, 5(1), pp. 44-56.

Houten, F.B., 1961. Origin of red-beds a review (1961-1972). Annual Review of Earth and Planetary Sciences, Vol. 1, pp. 39-61.

Johnsson, M.J., 1993. The system controlling the composition of clastic sediments: in Johnsson. In: Johnsson MJ, Basu A (eds) Processes controlling the composition of clastic sediments. Geological Society of America, Special Paper, Boulder, pp. 1-19.

Keller, W.D., 1970. Environmental aspects of clay minerals (Symposium on environmental aspects of clay minerals). Jour. Sed. Petrol., v. 40, pp.788-813.

Khater, H.M., El-Sabbagh, B.A., Fanny, M., Ezzat, M., Lottfy, M., and El Naggar, A.M., 2013. Effect of nano clay on alkali-activated water-cooled slag geopolymer. British J. of Applied Science and Technology, Vol. 3(4), pp.764-776.

Khoury, H.N., 2002. Clays and clay minerals in Jordan. Publications of the Deanship of Academic Research. The University of Jordan. Amman- Jordan.

Khoury, H.N., Hodali, H., Hourani, M., Mubarak, Y., Faqir, N., Hanayneh, B., and Esaifan, M., 2008. Mineral Polymerization of Some Industrial Rock and Minerals in Jordan. Publications of the Deanship of Academic Research. The University of Jordan. Amman-Jordan.

Kretz, R., 1983. Symbols for rock-forming minerals. American Mineralogist, 68, pp. 277-279.

Masoud, A.A., Ghristidis, G., and Koike, K., 2013. Characterization of El-Tih kaolin quality using mineralogical, geochemical, and geostatistical analyses. Clay Minerals, 48, pp. 1-20.

Melo, V., Singh, B., Schaefer, C., Novais, R., and Fontes, M., 2001. Chemical and mineralogical properties of kaolinite-rich Brazilian soils. Soil Sci. Soc. Am. J., 65, pp. 1324-1333.

Migdisove, A.A., 1960. On the titanium/aluminum ratios in sedimentary rocks. Geochemistry (U.S.S.R), English Transl., 2, pp. 178-194.

Millot, G., 1970. Geology of clays. Springer. Verlag, New York, 429 P.

Montes, C.R., Melfi, A.J., Carvalho, A., Vieira-Coelho, A.C., and Formoso, M.L.L 2002. Genesis, mineralogy, and geochemistry of kaolin deposits of the Jari River, Amapa State, Brazil. Clays and Clay Min., Vol. 50(4), pp. 494-503.

Murray, H.H., 2007. Applied Clay Mineralogy. Developments in Clay Science, 2, Elsevier, Amsterdam, 180 P.

Murray, H.H., and Keller, W.D., 1993. Kaolin and kaolin's., in Kaolin Genesis and Utilization (Murray, H.H., Bundy, W., and Harvey, C., editors). The Clay Minerals Society, Special Publication, 1, Boulder, Colorado, USA, pp. 1-24.

Nesbitt, H.W., and Young, G.M., 1982. Early Proterozoic climates and plate motions inferred from major element chemistry of lutites. Nature, 299, pp. 715-717.

Nesbitt, H.W., and Young, G.M., 1984. Prediction of some weathering trends of plutonic and volcanic rocks based on thermodynamic and kinetic considerations. Geochimica et Cosmochimica Acta, 48, pp. 1523-1534.

Nesbitt, H.W., and Young, G.M., 1989. Formation and diagenesis of weathering profiles. Journal of Geology, 97, pp. 129-147.

Nesbitt, H.W., Fedo, C.M., and Young, G.M., 1997. Quartz and feldspar stability, steady and non-steady state weathering, and petrogenesis of siliciclastic sands and muds. Journal of Geology, Vol. 105, pp. 173-191.

Okunlola, O., and Idowu, O., 2012. The geochemistry of claystone-shale deposits from the Maastrichtian Patti formation, Southern Bida basin, Nigeria. J. Earth Sci., v. 16(2), pp. 57-67.

Palache, C., Berman, H., and Frondel, C., 1951. Dana's system of mineralogy, (7th edition), Wiley publisher, v. II, pp. 208-217 and 482-486.

Pedersen, B.F., and Semmingsen, D., 1982. Neutron diffraction refinement of the structure of gypsum, CaSO4.2H2O. Acta Cryst., V0l. 38, pp. 1074-1077.

Perri, F., 2014. Oral communication composition, provenance, and source weathering of Mesozoic sandstones from Western-Central Mediterranean Alpine Chains. J. Afr. Earth Sci., Vol. 91, pp. 32-43.

Pruett, R.J., and Pickering, J., 2006. Kaolin. in: Industrial Minerals and Rocks (J. Elzea Kogel, N.C. Trivedi, J.M. Barker, and S.T. Krukowski, editors). Society for Mining, Metallurgy, and Exploration. Inc., Littleton, Colorado, U.S.A., pp. 390-427.

Railsback, L.B., 2003. An earth scientist's periodic table of the elements and their ions. Geology. 31, pp. 737-740.

Rankama, K., and Sahama, T.G., 1950. Geochemistry. Univ., Chicago Press, 912 P.

Roaldest, E., 1978. Mineralogical and chemical changes during weathering, transportation, and sedimentation in different environments with particular references to the distribution of Yttrium and lanthanide elements. Ph.D. Thesis, Geol. Inst., Univ. of Oslo, Norway.

Roser, B.P., and Korsch, R.J., 1986. Determined tectonic setting of sandstone-mudstone suites using SiO_2 content and K_2O/Na_2O ratio. J. Geology, 94, pp. 635-660.

Roy, P.D., Caballero, M., Lozano, R., and Smykatz-Kloss, W. 2008. Geochemistry of Late Quaternary sediments from Tecocomulco lake, central Mexico; implication to chemical weathering and provenance; Chemie der Erde, Geochemistry, Vol. 68, pp. 383-393.

Saber, E., Ali, M., and El-Sheikh, A., 2018. Provenance studies of Kalabsha kaolin deposits, Egypt: a petrographical and geochemical approach. Arabian J. Geos., Vol. 11(339), 15 P.

Said, R., 1962. The Geology of Egypt. Elsevier Publ. Comp, Amsterdam, 377 P.

Sayin, S.A., 2007. Origin of Kaolin Deposits: Evidence from the HisarcÝk (Emet-K.tahya) Deposits, Western Turkey. Turkish J Earth Sci., Vol. 16, pp. 77-96.

Schneider, R., Price, B., Muller, P., Kroon, D., and Alexander, I., 1997. Monsoon-related variations in Zaire (Congo) sediment load and influence of fluvial silicate supply on marine productivity in the east equatorial Atlantic during the last 200,000 years. Paleoceanography, Vol. 12(3), pp. 463-481.

Schroeder, P.A., Pruett, R.J. and Mealear, N.D., 2004. Crystal-chemical changes in an oxidative weathering front in a Georgia kaolin deposit. Clays and Clay Minerals, 52, pp. 211-220.

Suttner, L.J., and Dutta, P.K., 1986. Alluvial sandstone composition and paleoclimate; 1. Framework mineralogy. J. Sed. Pet., 56(3), pp. 329-345.

Taylor, S.R., and McLennan, S.M., 1985. The continental crust: its composition and evolution. 1st ed. Blackwell Scientific Publishers, Oxford, 312 P.

Tucker, M.E., 1981. Sedimentary petrology: An introduction. Blackwell Scientific Publications, London, pp. 40-189.

Wang, Z.W., Wang, J., Fu, X.G., Feng, X., Wang, D., Song, C.Y., Chen, W.B., and Zeng, S.Q., 2017. Petrography and geochemistry of Upper Triassic Sandstones from the Tumengela Formation in the Woruo Mountain area, North Qiangtang Basin, Tibet: implications for provenance, Source Area Weathering, and Tectonic Setting. Island Arc (John Wiley and Sons Australia, Ltd) 26(4), 15 P. https://doi.org/10.1111/iar.12191.

Whitney, D., and Evans, B.W., 2010. Abbreviation for names of rock-forming minerals. American Mineralogist, 95, pp. 185-187.

Wilson, I.R., 2004. Kaolin and halloysite deposits of China. Clay Minerals, 39, pp. 1-15.

Wronkiewicz, D.J., and Condie, K.C., 1987. Geochemistry of Archean shales from the Witwatersrand Supergroup, South Africa: source-area weathering and provenance. Geochim. Cosmochim. Acta, Vol. 51, pp. 2401-2416.

Youssef, E.A., 1996. Sedimentological studies on the central Wadi Kalabsha kaolin deposits, southwest of Aswan, Egypt. J. Mineral Petrol. Econ. Geol., Vol. 91, pp. 353-363.

Zhang, L., Gao, J., and Wang, Z.X., 2001. Low-temperature eclogite facies metamorphism in western Tianshan, Xinjiang. Science in China, Series D, Vol. 44, pp. 85-97.